Physica B 521 (2017) 361–364

Contents lists available at ScienceDirect

Physica B

journal homepage: www.elsevier.com/locate/physb

Theoretical Compton profile of diamond, boron nitride and carbon nitride

Julio C. Aguiar[a,*], Carlos R. Quevedo[b], José M. Gomez[b,c], Héctor O. Di Rocco[d,e]

[a] Autoridad Regulatoria Nuclear, Av. Del Libertador 8250, C1429BNP Buenos Aires, Argentina
[b] Universidad Nacional de Asunción, Facultad de Ciencias Exactas y Naturales, (CC1039), Campus Universitario de San Lorenzo, Paraguay
[c] Universidad Nacional de Asunción, Facultad Politécnica, (CC2111), Campus Universitario de San Lorenzo, Paraguay
[d] Instituto de Física "Arroyo Seco", Facultad de Ciencias Exactas, Universidad Nacional del Centro de la Provincia de Buenos Aires, Pinto 399, 7000 Tandil, Argentina
[e] Consejo Nacional de Investigaciones Científicas y Técnicas (CONICET), Argentina

ARTICLE INFO

Keywords:
Compton profile
Generalized gradient approximation
Diamond
Boron nitride and Carbon nitride

ABSTRACT

In the present study, we used the generalized gradient approximation method to determine the electron wave functions and theoretical Compton profiles of the following super-hard materials: diamond, boron nitride (*h*-BN), and carbon nitride in its two known phases: βC_3N_4 and gC_3N_4. In the case of diamond and *h*-BN, we compared our theoretical results with available experimental data. In addition, we used the Compton profile results to determine cohesive energies and found acceptable agreement with previous experiments.

1. Introduction

The so-called super-hard materials, especially carbon, boron and nitrogen compounds, have been extensively studied. The structural bonding of these elements presents remarkable properties such as: high temperature resistance, wear-resistant coatings, compressibility, high thermal conductivity, and low density. These properties allow creating abrasive tools, cutting tools, electronic components, and optical parts [1,2].

Among super-hard materials, diamond has the highest hardness and thermal conductivity. These properties determine greater industrial application in cutting and polishing tools. Gem diamond has a density of 3.513 g/cm^3 and an atomic weight of 12.01 amu with face centered cubic (*fcc*) crystal structure where the lattice constant a = 3.5669 Å in space group (227) and the Hermann–Mauguin notation is *Fd*3*m* [3].

Another hard material is boron nitride (*h*-BN), which has hexagonal form and a structure similar to that of graphite (space group (194) *P*63/*mmc*), where a = 2.504 Å and c = 6.661 Å, density = 2.18 g/cm^3, and atomic weight = 25.0124 amu [4].

Carbon nitride is also a hard material with has a structure equivalent to that of βSi_3N_4. In 1989, Liu and Cohen predicted the theoretical properties of βC_3N_4 by using an empirical model and local-density approximation (LDA) [5,6]. These authors showed that the bulk modulus of the hypothetical βC_3N_4 solid (~437 *mGPa*) could have a hardness comparable to that of diamond (442–446 GPa) with equivalent electronic densities. Other authors have predicted that the bandgap of βC_3N_4 are high (3–4 eV) [7–13]. The polycrystalline hexagonal lattice of βC_3N_4 (space group P63/m) has been experimentally determined to be a = 6.36 Å, and c = 2. 324 Å, whereas that of (C_3N_4 in graphitic phase gC_3N_4) (P6m2(187)) have been theoretically determined by using density-functional theory (DFT)-LDA, to be a = 4.74 Å, and c = 6.72Å with a density of ~2.3 g/cm^3 [10,14].

In the last decades, DFT has been widely used as a theoretical framework to calculate the electronic structure of atoms, molecules and solids [15,16]. On the other hand, LDA has provided a remarkably successful description for many electronic systems such as atomic, molecular and solid-state systems. However, in some applications where it is necessary to determine the wave functions, as in the case of Compton profile calculations, LDA shows that the profile is overestimated at low momentum transfer and underestimated around the Fermi momentum value. This failure has been attributed to the deficiency of LDA to describe the electronic exchange and correlation effects. A method that allows including the neglected exchange and correlation effects in LDA is the Lam–Platzman correction (LPC) [17–19]. This correction of the momentum density resolves the residual discrepancies outlined above and facilitates a critical assessment of Compton profiles. Recently, a semi-empirical method based on the joint use of the Fermi liquid model and Hartree–Fock formalism, has been proposed to include the effects of electron correlation [20].

In the present study, we were interested in the ability of the generalized gradient approximation (GGA) proposed by Perdew, Burke and Ernzerhof (PBE) [21] to describe the electron momentum density and isotropic Compton profile for diamond, *h*-BN, βC_3N_4 and

* Corresponding author.
E-mail address: jaguiar@arn.gob.ar (J.C. Aguiar).

http://dx.doi.org/10.1016/j.physb.2017.07.016
Received 25 January 2017; Received in revised form 24 May 2017; Accepted 7 July 2017
Available online 08 July 2017
0921-4526/

g-C_3N_4 by applying self-consistent solutions of the Schrö dinger–Kohn–Sham non–relativistic equations, under Troullier and Martins (TM) schemes [22]. The Compton profile allows verifying the quality of the electron wave functions through Fourier transforms, defining the Fermi surface and verifying the quality of band structure calculations [23,24]. Compton profiles using these types of calculations have been previously reported for Be, Al, Ti, TiO2 and ZnO [25–27]. Diamond and *h*-BN have been widely studied both theoretically and experimentally by Compton profiles [28–35]. In contrast, no Compton profile calculations have yet been reported for carbon nitride.

2. Computational procedures

One-electron wave functions for diamond, *h*-BN, β-C_3N_4 and g-C_3N_4 are calculated within the impulse approximation of the form

$$\psi_{nlm}(r, \theta, \phi) = R_{nl}(r) Y_l^m(\theta, \phi), \tag{1}$$

where the atomic radial wave functions $R_{nl}(\mathbf{r})$ for core electrons, the norm-conserving pseudo-potentials, and the pseudo-atomic orbitals for valence electrons are obtained using the ADPACK code [36]. The pseudo-potentials and orbitals are used as primitive basis input data for the execution of the OPENMX program (Open source package for Material eXplorer), which allows determining the Bloch wave functions of crystalline solids in the unit cell [37–40]. The norm-conserving pseudo-potentials contain a charge density $\rho(\mathbf{r}) = \sum |R_{nl}(r)|^2 r^2$ by orbital l constructed by standard schemes from all electron calculations. Assuming spherical screening, the Schrödinger–Kohn–Sham non-relativistic equations under the GGA functional can be given by

$$\left[-\frac{1}{2}\frac{\partial^2}{\partial r^2} + \frac{l(l+1)}{2r^2} + V_l^{eff}[\rho, \mathbf{r}]\right]\mathbf{r}R_{nl}(\mathbf{r}) = \mathbf{r}R_{nl}(\mathbf{r})\varepsilon_{nl}. \tag{2}$$

The effective potentials V_l^{eff} can be decomposed into the local Hartree potential V_H, the non-local exchange-correlation (XC) potential due to the valence and core electrons, and V^{ext}, wich is the Coulomb potential of the nuclei:

$$V_l^{eff}[\rho, \mathbf{r}] = \int \frac{\rho(\mathbf{r}')}{|\mathbf{r} - \mathbf{r}'|} d\mathbf{r} + \frac{\partial E_{XC}[\rho]}{\partial \rho(\mathbf{r})} + V^{ext}(\mathbf{r}). \tag{3}$$

The ADPACK code allows including parameterizations of the LDA or GGA by using the exchange correlation energy

$$E_{XC}^{LDA}[\rho] = \int \rho(\mathbf{r}) \varepsilon_{XC}^{LDA}[\rho(\mathbf{r})] d^3r, \tag{4}$$

where

$$\varepsilon_{XC}^{LDA}[\rho(\mathbf{r})] = -\frac{3}{4}\left(\frac{3}{\pi}\right)^{1/3} \rho^{4/3}(\mathbf{r}). \tag{5}$$

In the case of GGA, the exchange-correlation functional depends on the density and its gradient as follows:

$$E_{XC}^{GGA}[\rho] = \int \rho(\mathbf{r}) \varepsilon_{XC}^{GGA}[\rho(\mathbf{r}), \nabla\rho(\mathbf{r})] d^3r. \tag{6}$$

An improvement of the LDA functional is the GGA-PBE [21], represented by

$$E_{XC}^{GGA}[\rho] = \int \varepsilon_{XC}^{LDA}[r_s(r)] F_{XC}[r_s(r), s(r)] d^3r, \tag{7}$$

where r_s is the Wigner-Seitz radius and is related to Fermi's momentum $r_s = 1.9192/k_F$. The function F_{XC} is given by

$$F_{XC}[r_s, s] = F_X[s] + F_C[r_s, s] \tag{8}$$

where

$$S = \frac{|\nabla\rho|}{2\rho k_F}, \tag{9}$$

and

$$F_X[s] = 0.804 - \frac{0.804}{1 + \frac{0.21951}{0.804} s^2}. \tag{10}$$

2.1. Compton profile

The isotropic Compton profile $J_{nl}(q)$ for the nl orbital is defined as the projection of the electron momentum density $\rho(p)$ along the scattering vector after the collision

$$J_{nl}(q) = \frac{1}{2}\int_{|q|}^{\infty} \sum |\chi_{nl}(p)|^2 p dp = \frac{1}{2}\int_{|q|}^{\infty} \rho(p) p dp, \tag{11}$$

where $\chi_{nl}(p)$ is called momentum space wave function and can be obtained via the Fourier transforms of $R_{nl}(r)$ according to

$$\chi_{nl}(p) = \left(\frac{2}{\pi}\right)^{1/2} (-i)^l \int_0^{\infty} R_{nl}(r) j_l(pr) r^2 dr, \tag{12}$$

where $j_l(pr)$ is the spherical Bessel function of the first kind, p is the momentum of the electron in the atom, and q is the projection of the momentum transfer $\mathbf{k}$ on the electron momentum $\mathbf{p}$ before collision:

$$q = -\frac{\mathbf{k}.\,\mathbf{p}}{k}. \tag{13}$$

2.2. Cohesive energy by Compton profile

The total ground-state energy E_T of electrons in crystals can be obtained from the solution to the Schrödinger equation in momentum space [41]. The expectation value of kinetic energy $\langle E_k \rangle \equiv p^2/2$ follows from the application of the virial theorem, which connects the expectation values of $\langle E_k \rangle$ and potential $\langle V \rangle$ energy of a system as follows:

$$\langle E_k \rangle = -\langle E_T \rangle = -\langle V \rangle/2. \tag{14}$$

The application of the virial theorem allows determining the $\langle E_k \rangle$ of an isotropic system via

$$\langle E_k \rangle = \frac{3}{2}\int_0^{\infty} \sum J_{nl}(q) q^2 dq. \tag{15}$$

Additionally, it is possible to determine the cohesive energy from the differences between calculated free-atomic $J(q)_{atom}$ and $J(q)_{crystal}$ in crystalline solids. Thus, cohesive energy $E_{coh/atom}$ is defined as the difference between the total ground-state energy of the Compton profile of the crystal and the sum of the individual atoms, as follows:

$$E_{coh/atom} = \frac{1}{2}\int_0^{\infty} [J(q)_{crystal} - J(q)_{atom}] q^2 dq. \tag{16}$$

The values of $J(q)_{atom}$ can be obtained from Hartree-Fock Compton profile calculations [42], and the values of $J(q)_{crystal}$ can be measured or calculated. In the present case, the values of $J(q)_{crystal}$ are obtained from the present GGA-PBE-TM scheme and those of $J(q)_{crystal}$ are determined via Hartree-Fock wave functions by using Fischer's code [43]. The application of this method has the advantage that at high values of q, where the contribution is limited to the core electrons, the integral is small, whereas at low values of q, the integral is significant.

3. Results and discussion

In all cases, the valence states were expanded over s–, p–, and d–like character where the valence electron densities distribution obtained from tabulated radial GGA-PBE wave functions are shown in Fig. 1. The Monkhorst-Pack k-point grid used were $3 \times 3 \times 3$ for diamond, $20 \times 20 \times 1$ for *h*-BN, $3 \times 3 \times 8$ for β-C_3N_4 and $6 \times 6 \times 4$ for g-C_3N_4.

To facilitate comparison between the different structures, the radial valence electron density was normalized to units according to

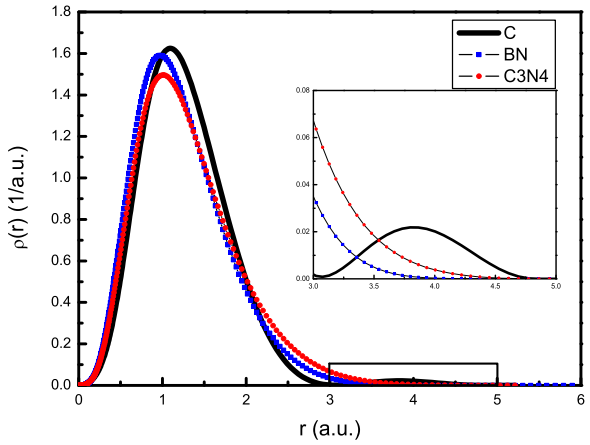

Fig. 1. Radial valence electron density; the black solid curve denotes diamond, the solid blue squares denote *h*-BN; and the red solid circles denote βC_3N_4. Inset: values of the densities in the ranging from 3 to 5 a.u. (For interpretation of the references to color in this figure legend, the reader is referred to the web version of this article.)

$$\rho(r) = \int_0^\infty [R_{nl}^{GGA}(r)]^2 r^2 dr. \quad (17)$$

In the case of diamond, the presence of one prominent hump of 1.62 at 1.10 a.u. of the center and another one 3.9 a.u is the result of the strongly attractive C 2*p* potential of the purely covalent diamond. In *h*-BN, the valence electron density is strongly localized near the N and exhibits only a single peak of height 1.60 at 0.96 a.u. In the case of βC_3N_4 a hump of 1.50 at 0.99 of the center is observed. Thus, the heteropolarity of the C-N bond in βC_3N_4 lies intermediate between purely covalent diamond and partially ionic boron nitride.

The theoretical Compton profiles Table 1 were compared with previous experiments for diamond Fig. 2 [29] and hBN Fig. 3 [31]. The differences between βC_3N_4 and gC_3N_4 are shown in Fig. 4.

3.1. Diamond

We assumed that the solid bulk has a face-centered cubic structure, where by minimization of the energy, the lattice constant is determined to be $a = 3.4969$ Å and the experimental value is $a = 3.5669$ Å. The Brillouin zone determined by k-point sampling grids on super cell size was 3×3x3. The cohesive energy of diamond computed via the theoretical Compton profile data using Eq. (16) is −0.2612 a.u./atom, being the experimental value −0.271 a.u./atom [44]. The difference between the experimental Compton profile for diamond and our calculations is shown in Fig. Fig. 2.

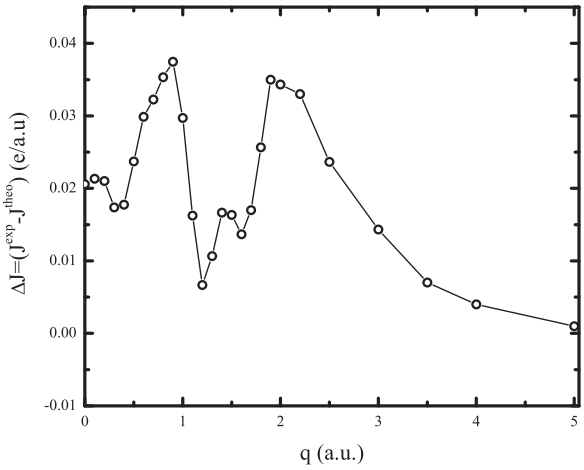

Fig. 2. Empty circles denote differences between experimental Compton profiles of Reed and Eisenberger [29] and our GGA-PBE calculations [$\Delta J = J^{exp} - J^{theo}$]. The size of the circles corresponds to the experimental resolution, which is less than 0.4 a.u.

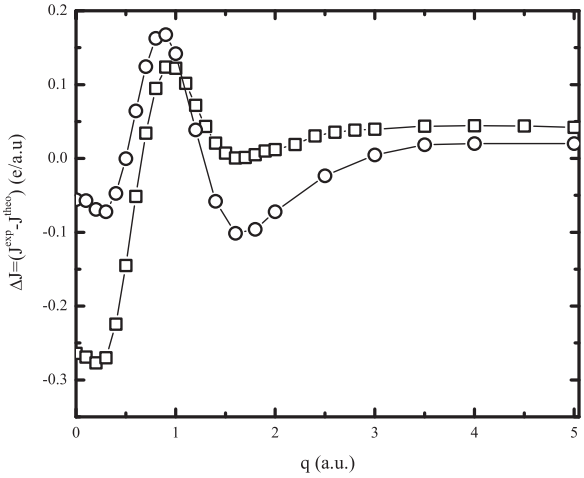

Fig. 3. Squares denote differences in the Compton profiles between our approach (GGA-PBE) and previous experimental results for*h*-BN [35]. Circles denote our approximation and previous experimental results [31].

3.2. h-BN

The hexagonal boron nitride form of *h*-BN was determined as a structure similar to that of graphite, where the lattice constants

Table 1
Isotropic Compton profile calculations for diamond,*h*-BN, βC_3N_4 andgC_3N_4 obtained by using GGA-PBE schemes normalized to 2.90, 5.86, 6.34 electrons equal to the area under 0 to+ 7 a.u., respectively.

q (a.u)	Diamond	*h*-BN	βC_3N_4	gC_3N_4	*q* (a.u)	Diamond	*h*-BN	βC_3N_4	gC_3N_4
0.0	2.0667	4.4339	4.7378	4.7490	1.6	0.4590	1.0592	1.1653	1.1627
0.1	2.0581	4.4180	4.7032	4.7140	1.7	0.4005	0.9427	1.0401	1.0379
0.2	2.0321	4.3629	4.6023	4.6121	1.8	0.3562	0.8431	0.9334	0.9318
0.3	1.9887	4.2511	4.4395	4.4477	1.9	0.3224	0.7579	0.8427	0.8415
0.4	1.9271	4.0655	4.2232	4.2294	2.0	0.2964	0.6872	0.7652	0.7643
0.5	1.8490	3.8122	3.9634	3.9673	2.2	0.2584	0.5740	0.6393	0.6399
0.6	1.7538	3.5015	3.6736	3.6752	2.4	0.2313	0.4906	0.5453	0.5458
0.7	1.6437	3.1616	3.3647	3.3642	2.6	0.2103	0.4225	0.4698	0.4702
0.8	1.5208	2.8212	3.0475	3.0452	2.8	0.1937	0.3688	0.4103	0.4105
0.9	1.3886	2.5003	2.7373	2.7336	3.0	0.1796	0.3233	0.3602	0.3602
1.0	1.2513	2.2110	2.4397	2.4352	3.5	0.1497	0.2373	0.2669	0.2670
1.1	1.1150	1.9531	2.1614	2.1565	4.0	0.1203	0.1768	0.2010	0.2011
1.2	0.9432	1.7262	1.9086	1.9038	4.5	0.0903	0.1321	0.1521	0.1521
1.3	0.7811	1.5258	1.6826	1.6782	5.0	0.0640	0.0989	0.1150	0.1150
1.4	0.6450	1.3492	1.4843	1.4804	6.0	0.0338	0.0559	0.0664	0.0664
1.5	0.5353	1.1936	1.3125	1.3093	7.0	0.0210	0.0315	0.0377	0.0377

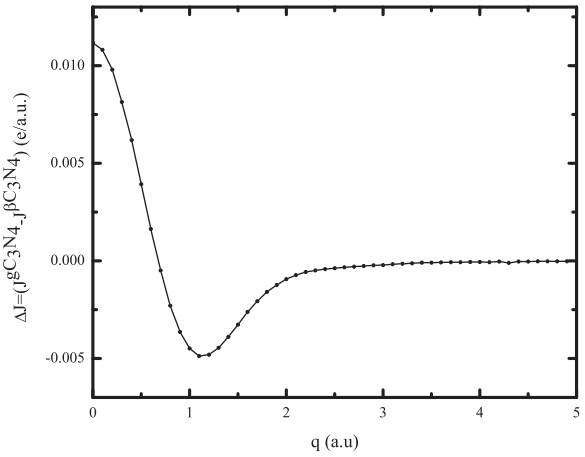

Fig. 4. Circles denote the differences in the Compton profiles betweengC_3N_4 and βC_3N_4.

determined by minimization of the energy are $a = 2.5528$ Å and $c = 6.7905$ Å, and where experimental values are $a = 2.504$ Å and $c = 6.661$ Å. The cohesive energy of diamond was computed via the theoretical Compton profile, where the value found was −0.2379 a.u./atom, being the experimental value −0.2425 a.u./atom [45]. The difference between the experimental Compton profiles for *h*-BN and our calculations is shown in Fig. Fig. 3.

3.3. βC_3N_4 and gC_3N_4

The polycrystalline hexagonal lattice of βC_3N_4 has been theoretically determined to be $a = 6.3937$ Å and $c = 2.2055$ Å, whereas for gC_3N_4 the equilibrium structural parameters theoretically determined using GGA-PBE were $a = 4.7458$ Å and $c = 6.7258$ Å. The Cohesive energy of βC_3N_4 was computed via the theoretical Compton profile, where the value found was −0.2076 a.u./atom, being −0.2131 a.u./atom the value predicted by Liu and Cohen [5,6]. The differences between our theoretical Compton profiles for βC_3N_4 andgC_3N_4 are shown in Fig. Fig. 4.

The differences observed between the Compton profiles of βC_3N_4 andgC_3N_4 show that the electron momentum density distributions have different electronic behavior, probably attributable to the strong anitropy of the two phases.

4. Conclusions

The structural and electronic properties of diamond, hexagonal boron nitride (*h*-BN) and carbon nitride in its two known phases (βC_3N_4 andgC_3N_4) were calculated from all-electron wave functions. Good agreement between cohesive energies and Compton profile experiments was observed in all cases. With respect to the structural properties of diamond, we were able to reproduce the experimental values for the cohesive energy within 3%. This proves the excellent capability of the generalized gradient approximation to calculate the electronic properties of covalent such as diamond and semi-ionic materials (BN and C_3N_4). In addition, we demonstrated that the Compton profile of diamond can be estimated with relative accuracy (1–5%) when compared to experimental results. However, the results obtained for*h*-BN were not good when compared with previous experiments performed by Tyk et al. [35], but showed excellent agreement with those performed by*h*-BN Ahuja et al. [31]. According to DFT theory, the valence electrons density allows describing all the physical and chemical properties of the material. Consequently, wave functions calculations allow comparing these covalent solids. Thus, we concluded that h-BN and Carbon Nitride have a similar behavior in contradistinction to the diamond (see Fig. 1). In summary, our study of the electronic properties of diamond, boron nitride and carbon nitride via the Compton profile offers additional information of these materials, such as the fact that βC_3N_4 andgC_3N_4 show small differences, probably attributable to the strong anitropy of the two phases.

Acknowledgments

We thank the support from Universidad Nacional del Centro de la Provincia de Buenos Aires (UNCPBA, Argentina), the Universidad Nacional de Asunción (UNA-FaCEN, Paraguay) and the Nuclear Regulatory Authority of Argentina.

References

[1] E. Yasuda, M. Inagaki, K. Kaneko, M. Endo, A. Oya, and Y. Tanabe (Eds), Carbon Alloys: Novel Concept to Develop Carbon Science and Technology, 1st ed., Elsevier Science Ltd. UK, (2003) pp. 545–558.
[2] G. Dong, Y. Zhang, Q. Pan, J. Qiu, J. J. Photochem. Photobiol., C 20 (2014) 33.
[3] D.R. Lide (Ed.), CRC Handbook of Chemistry and Physics, 89th ed. (CRC Press, Boca Raton, 2009).
[4] R.W.G. Wyckoff, Cryst. Struct. 1 (1963) 85.
[5] A.Y. Liu, M.L. Cohen, Science 245 (1989) 841.
[6] A.Y. Liu, M.L. Cohen, Phys. Rev. B 41 (1990) 10727.
[7] J.L. Corkill, M.L. Cohen, Phys. Rev. B 48 (1993) 17622.
[8] A. Reyes-Serrato, D.H. Galván, I.L. Garzón, Phys. Rev. B 52 (1995) 6293.
[9] A.H. Reshak, S. Ayaz Khan, S. Auluck, RSC Adv. 4 (2014) 6957.
[10] D.M. Teter, R.J. Hemley, Science 271 (1996) 53.
[11] Y. Fahmy, T.D. Shen, D.A. Tucker, R.L. Spontak, C.C. Koch, J. Mater. Res. 14 (1999) 2488.
[12] A. Thomas, A. Fischer, F. Goettmann, M. Antonietti, Jens-Oliver Müller, R. Schlögl, J.M. Carlsson, J. Mater. Chem. 18 (2008) 4893.
[13] J. Wei, J. Appl. Phys. 89 (2001) 4099.
[14] Long-Wei Yin, Mu-Sen Li, Yu-Xian Liu, Jin-Ling Sui, Jing-Min Wang, J. Phys.:Condens. Matter 15 (2003) 309.
[15] P. Hohenberg, W. Kohn, Phys. Rev. 136 (1964) B864.
[16] W. Kohn, L.S. Sham, Phys. Rev. 140 (1965) A1133.
[17] L. Lam, P. Platzman, Phys. Rev. B 9 (1974) 5122.
[18] D.A. Cardwell, M.J. Cooper, J. Phys. Condens. Matter 1 (1989) 9357.
[19] B. Barbiellini, A. Bansil, J. Phys. Chem. Solids 62 (2001) 2181.
[20] Julio C. Aguiar, Darío Mitnik, Héctor O. Di Rocco, J. Phys. Chem. Solids 83 (2015) 64.
[21] J.P. Perdew, K. Burke, M. Ernzerhof, Phys. Rev. Lett. 77 (1996) 3865.
[22] N. Troullier, J.L. Martins, Phys. Rev. B, 4, 3, 1991, 1993.
[23] B.G. Williams, (Ed.), Compton Scattering, McGraw-Hill, New York, 1977.
[24] M.J. Cooper, (Ed.), X-Ray Compton Scattering, Oxford University Press, New York, 2004.
[25] Julio C. Aguiar, Héctor O. Di Rocco, Darío Mitnik, 74 (2013) 1341.
[26] S.P. Limandri, R.C. Fadanelli, M. Behar, L.C.C.M. Nagamine, J.M. Fernández-Varea, I. Abril, R. Garcia-Molina, C.C. Montanari, J.C. Aguiar, D. Mitnik, J.E. Miraglia, N.R. Arista, Eur. Phys. J. D 68 (2014) 194.
[27] R.C. Fadanelli, C.D. Nascimento, C.C. Montanari, J.C. Aguiar, D. Mitnik, A. Turos, E. Guziewicz, M. Behar, Eur. Phys. J. D 70 (2016) 178.
[28] R.J. Weiss, Philos. Mag. 29 (1974) 1029.
[29] W.A. Reed, P. Eisenberger, Phys. Rev. B 6 (1972) 4596.
[30] R. Dovesi, C. Pisani, C. Roetti, P. Dellarole, Phys. Rev. B 24 (1981) 4170.
[31] B.L. Ahuja, Anil Gupta, B.K. Sharma, Z. Nat. 48a (1993) 310.
[32] R.J. Weiss, Phys. Rev. 176 (1968) 900.
[33] D. Ayma, M. Rérat, A. Lichanot, J. Phys.: Condens. Matter 10 (1998) 557.
[34] G.G. Wepfer, R.N. Euwema, G.T. Surratt, D.L. Wilhite, Phys. Rev. B 9 (1974) 2670.
[35] R. Tyk, J. Felsteiner, I. Gertner, Phys. Rev. B 32 (1985) 2625.
[36] http://www.openmx-square.org.
[37] T. Ozaki, Phys. Rev. B 67 (2003) 155108.
[38] T. Ozaki, H. Kino, Phys. Rev. B 69 (2004) 195113.
[39] M. Toyoda, T. Ozaki, Phys. Rev. A 83 (2011) 032515.
[40] T. Ozaki, M. Toyoda, Comput. Phys. Commun. 182 (2011) 1245.
[41] R. Epstein, Phys. Rev. A. 8 (1973) 160.
[42] F. Biggs, L.B. Mendelsohn, J.B. Mann, At. Data Nucl. Data Tables 16 (1975) 201.
[43] C.F. Fischer, Comp. Phys. Commun. 64 (1991) 369.
[44] James R. Chelikowsky, Steven G. Louie, Phys. Rev. B 29 (1984) 3470.
[45] Renata M. Wentzcovitch, K.J. Chang, Marvin L. Cohen, Phys. Rev. B 34 (1986) 1071.